Search for the $b \to d\gamma$ process

D. Mohapatra,[47] M. Nakao,[7] B. D. Yabsley,[47] K. Abe,[7] K. Abe,[40] H. Aihara,[42] K. Arinstein,[1] Y. Asano,[46] T. Aushev,[11] T. Aziz,[38] S. Bahinipati,[4] A. M. Bakich,[37] E. Barberio,[18] M. Barbero,[6] I. Bedny,[1] U. Bitenc,[12] I. Bizjak,[12] A. Bondar,[1] A. Bozek,[24] M. Bračko,[7,49,12] J. Brodzicka,[24] T. E. Browder,[6] Y. Chao,[23] A. Chen,[21] W. T. Chen,[21] B. G. Cheon,[3] R. Chistov,[11] S.-K. Choi,[5] Y. Choi,[36] A. Chuvikov,[32] J. Dalseno,[18] M. Danilov,[11] M. Dash,[47] J. Dragic,[7] S. Eidelman,[1] T. Gershon,[7] G. Gokhroo,[38] B. Golob,[17,12] A. Gorišek,[12] T. Hara,[29] K. Hayasaka,[19] M. Hazumi,[7] L. Hinz,[16] T. Hokuue,[19] Y. Hoshi,[40] S. Hou,[21] W.-S. Hou,[23] Y. B. Hsiung,[23] T. Iijima,[19] K. Ikado,[19] A. Imoto,[20] K. Inami,[19] A. Ishikawa,[7] M. Iwasaki,[42] Y. Iwasaki,[7] J. H. Kang,[48] J. S. Kang,[14] H. Kawai,[2] T. Kawasaki,[26] H. R. Khan,[43] H. J. Kim,[15] S. M. Kim,[36] K. Kinoshita,[4] P. Križan,[17,12] P. Krokovny,[1] R. Kulasiri,[4] C. C. Kuo,[21] A. Kuzmin,[1] Y.-J. Kwon,[48] G. Leder,[10] S. E. Lee,[34] T. Lesiak,[24] J. Li,[33] A. Limosani,[7] S.-W. Lin,[23] D. Liventsev,[11] G. Majumder,[38] F. Mandl,[10] A. Matyja,[24] Y. Mikami,[41] W. Mitaroff,[10] H. Miyata,[26] G. R. Moloney,[18] T. Nagamine,[41] Y. Nagasaka,[8] E. Nakano,[28] H. Nakazawa,[7] S. Nishida,[7] O. Nitoh,[45] T. Nozaki,[7] S. Ogawa,[39] T. Ohshima,[19] S. Okuno,[13] S. L. Olsen,[6] Y. Onuki,[26] W. Ostrowicz,[24] H. Ozaki,[7] P. Pakhlov,[11] H. Park,[15] R. Pestotnik,[12] L. E. Piilonen,[47] Y. Sakai,[7] T. R. Sarangi,[7] N. Sato,[19] N. Satoyama,[35] T. Schietinger,[16] O. Schneider,[16] J. Schümann,[23] A. J. Schwartz,[4] K. Senyo,[19] M. E. Sevior,[18] H. Shibuya,[39] A. Somov,[4] N. Soni,[30] R. Stamen,[7] S. Stanič,[27] M. Starič,[12] T. Sumiyoshi,[44] F. Takasaki,[7] K. Tamai,[7] N. Tamura,[26] M. Tanaka,[7] G. N. Taylor,[18] Y. Teramoto,[28] X. C. Tian,[31] K. Trabelsi,[6] S. Uehara,[7] T. Uglov,[11] K. Ueno,[23] S. Uno,[7] G. Varner,[6] S. Villa,[16] C. C. Wang,[23] C. H. Wang,[22] Y. Watanabe,[43] Q. L. Xie,[9] Y. Yamashita,[25] M. Yamauchi,[7] Heyoung Yang,[34] J. Ying,[31] C. C. Zhang,[9] J. Zhang,[7] L. M. Zhang,[33] Z. P. Zhang,[33] V. Zhilich,[1] and D. Zürcher[16]

(The Belle Collaboration)

[1] *Budker Institute of Nuclear Physics, Novosibirsk*
[2] *Chiba University, Chiba*
[3] *Chonnam National University, Kwangju*
[4] *University of Cincinnati, Cincinnati, Ohio 45221*
[5] *Gyeongsang National University, Chinju*
[6] *University of Hawaii, Honolulu, Hawaii 96822*
[7] *High Energy Accelerator Research Organization (KEK), Tsukuba*
[8] *Hiroshima Institute of Technology, Hiroshima*
[9] *Institute of High Energy Physics, Chinese Academy of Sciences, Beijing*
[10] *Institute of High Energy Physics, Vienna*
[11] *Institute for Theoretical and Experimental Physics, Moscow*
[12] *J. Stefan Institute, Ljubljana*
[13] *Kanagawa University, Yokohama*
[14] *Korea University, Seoul*
[15] *Kyungpook National University, Taegu*
[16] *Swiss Federal Institute of Technology of Lausanne, EPFL, Lausanne*
[17] *University of Ljubljana, Ljubljana*
[18] *University of Melbourne, Victoria*
[19] *Nagoya University, Nagoya*
[20] *Nara Women's University, Nara*
[21] *National Central University, Chung-li*
[22] *National United University, Miao Li*
[23] *Department of Physics, National Taiwan University, Taipei*
[24] *H. Niewodniczanski Institute of Nuclear Physics, Krakow*
[25] *Nippon Dental University, Niigata*
[26] *Niigata University, Niigata*
[27] *Nova Gorica Polytechnic, Nova Gorica*
[28] *Osaka City University, Osaka*
[29] *Osaka University, Osaka*
[30] *Panjab University, Chandigarh*
[31] *Peking University, Beijing*
[32] *Princeton University, Princeton, New Jersey 08544*
[33] *University of Science and Technology of China, Hefei*
[34] *Seoul National University, Seoul*
[35] *Shinshu University, Nagano*
[36] *Sungkyunkwan University, Suwon*
[37] *University of Sydney, Sydney NSW*

[38] Tata Institute of Fundamental Research, Bombay
[39] Toho University, Funabashi
[40] Tohoku Gakuin University, Tagajo
[41] Tohoku University, Sendai
[42] Department of Physics, University of Tokyo, Tokyo
[43] Tokyo Institute of Technology, Tokyo
[44] Tokyo Metropolitan University, Tokyo
[45] Tokyo University of Agriculture and Technology, Tokyo
[46] University of Tsukuba, Tsukuba
[47] Virginia Polytechnic Institute and State University, Blacksburg, Virginia 24061
[48] Yonsei University, Seoul
[49] University of Maribor, Maribor

(Dated: May 30 2005)

We report the results of a search for the flavor-changing neutral current process $b \to d\gamma$ using a sample of 275 million B meson pairs accumulated by the Belle detector at KEKB. We find no significant signal for the exclusive decays $B^- \to \rho^-\gamma$, $\overline{B}^0 \to \rho^0\gamma$, or $\overline{B}^0 \to \omega\gamma$. Assuming an isospin relation between the three modes, we set an upper limit for the combined branching fraction $\mathcal{B}(B \to (\rho,\omega)\gamma)$, of 1.4×10^{-6} at the 90% confidence level. This limit can be used to constrain the ratio of CKM matrix elements $|V_{td}/V_{ts}|$.

PACS numbers: 11.30.Hv, 13.40.Hq, 14.65.Fy, 14.40.Nd

The $b \to d\gamma$ process, shown in Fig. 1(a), is a flavor changing neutral current transition that proceeds via loop diagrams in the Standard Model (SM). It is suppressed with respect to $b \to s\gamma$ by the Cabibbo-Kobayashi-Maskawa (CKM) factor $|V_{td}/V_{ts}|^2 \sim 0.04$ with a large uncertainty due to the lack of precise knowledge of V_{td}. The exclusive modes $B \to \rho\gamma$ and $B \to \omega\gamma$, which are presumably the easiest modes to search for, have not yet been observed [1]. Calculations based on the measured rate for the $b \to s\gamma$ process $B \to K^*\gamma$ that include $|V_{td}/V_{ts}|^2$ suppression, corrections due to form factors, $SU(3)$ breaking effects, and, for B^- decay, the additional annihilation diagram of Fig. 1(b), predict branching fractions in the range $(0.9\text{–}2.7) \times 10^{-6}$ [2, 3]. Measurement of these exclusive branching fractions would improve the constraints on $|V_{td}/V_{ts}|$ in the context of the SM, and provide sensitivity to physics beyond the SM that is complementary to that from $b \to s\gamma$.

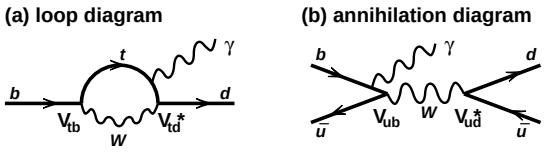

FIG. 1: (a) Loop diagram for $b \to d\gamma$ and (b) annihilation diagram for $B^- \to \rho^-\gamma$ only.

In this paper, we report the results of a search for the $b \to d\gamma$ process using a sample of (275 ± 3) million B meson pairs accumulated at the $\Upsilon(4S)$ resonance. The data are produced in e^+e^- annihilation at the KEKB energy-asymmetric (3.5 on 8 GeV) collider [4] and collected with the Belle detector [5]. The Belle detector includes a silicon vertex detector (SVD), a central drift chamber (CDC), aerogel threshold Cherenkov counters (ACC), time-of-flight (TOF) scintillation counters, and an electromagnetic calorimeter (ECL) comprised of CsI(Tl) crystals located inside a 1.5 T superconducting solenoid coil. An iron flux-return located outside of the coil is instrumented to identify muons (KLM). The dataset consists of two subsets: the first 152 million B meson pairs were collected with a 2.0 cm radius beampipe and a 3-layer SVD, and the remaining 123 million B meson pairs with a 1.5 cm radius beampipe, a 4-layer SVD and a small-cell inner drift chamber [6].

We reconstruct the following final states: $B^- \to \rho^-\gamma$, $\overline{B}^0 \to \rho^0\gamma$, and $\overline{B}^0 \to \omega\gamma$. Charge conjugate modes are implicitly included throughout this paper. We also reconstruct control samples of $B^- \to K^{*-}\gamma$ and $\overline{B}^0 \to \overline{K}^{*0}\gamma$ decays. The following decay chains are used to reconstruct the intermediate states: $\rho^- \to \pi^-\pi^0$, $\rho^0 \to \pi^+\pi^-$, $\omega \to \pi^+\pi^-\pi^0$, $K^{*-} \to K^-\pi^0$, $\overline{K}^{*0} \to K^-\pi^+$, and $\pi^0 \to \gamma\gamma$.

Photon candidates are reconstructed from isolated clusters in the ECL that have no corresponding charged track, and a shower shape that is consistent with that of a photon. A photon in the barrel region of the ECL ($33^\circ < \theta_\gamma < 128^\circ$ in the laboratory frame) with a center-of-mass (c.m.) energy in the range 1.8 GeV $< E^*_\gamma <$ 3.4 GeV is selected as the primary photon candidate. To suppress backgrounds from $\pi^0 \to \gamma\gamma$ and $\eta \to \gamma\gamma$ decays, we veto the event if the reconstructed mass of the primary photon and any other photon of energy 30 (200) MeV or more is within a $\pm 3\sigma$ window, i.e., ± 18 (± 32) MeV/c^2, around the π^0 (η) mass. This set of criteria is referred to as the π^0/η veto. For the primary photon, we sum the energy deposited in arrays of 3×3 and 5×5 ECL cells around

the maximum energy cell; if their ratio is less than 0.95, the event is vetoed.

Neutral pions are formed from photon pairs with invariant masses within ± 10 (16) MeV/c^2 of the nominal π^0 mass, corresponding to a $\sim 2\sigma$ ($\sim 3\sigma$) window for the $\rho^-\gamma$ and $K^{*-}\gamma$ ($\omega\gamma$) modes. The photon momenta are then recalculated with a π^0 mass constraint. We require the energy of each photon to be greater than 30 MeV. We also require the c.m. momentum of the π^0 to be greater than 0.5 GeV/c for the $\rho^-\gamma$ and $K^{*-}\gamma$ modes.

Charged pions and kaons are reconstructed as tracks in the CDC and SVD. Each track is required to have a transverse momentum greater than 100 MeV/c and distance of closest approach to the interaction point of less than 2 cm in radius and ± 5 cm along the z-axis, which is aligned opposite to the positron beam. We do not use the track to form the signal candidate if, when combined with any other track, it forms a K^0_S candidate with an invariant mass within ± 10 MeV/c^2 of the nominal K^0_S mass and a displaced vertex that is consistent with a K^0_S. We determine the pion (L_π) and kaon (L_K) likelihoods from ACC, CDC and TOF information, and form a likelihood ratio $L_\pi/(L_\pi + L_K)$ to separate pions from kaons. We select pions using criteria which have an efficiency of 89% and for which $\sim$10% of kaons are misidentified as pions. For the $\omega\gamma$ mode, we relax the requirement to select 94% of pions. (In the $K^*\gamma$ modes, we select kaons with an efficiency of 76–80%.) In addition, we remove tracks that are consistent with being electrons or muons.

Invariant masses for the ρ and ω candidates are required to be within windows of ± 150 MeV/c^2 and ± 30 MeV/c^2, respectively, around their nominal masses.

B candidates are reconstructed by combining a ρ or ω candidate and the primary photon using two variables: the beam-energy constrained mass $M_{\rm bc} = \sqrt{(E^*_{\rm beam}/c^2)^2 - |p^*_B/c|^2}$ and the energy difference $\Delta E = E^*_B - E^*_{\rm beam}$; p^*_B and E^*_B are the c.m. momentum and energy of the B candidate, and $E^*_{\rm beam}$ is the c.m. beam energy. The magnitude of the photon momentum is replaced by $(E^*_{\rm beam} - E^*_{\rho/\omega})/c$ when the momentum p^*_B is calculated. To optimize the event selection, we study Monte Carlo (MC) events in the region -0.10 GeV $< \Delta E < 0.08$ GeV and 5.273 GeV/c^2 $< M_{\rm bc} <$ 5.285 GeV/c^2: we choose selection criteria to maximize $N_S/\sqrt{N_B}$, where N_S is the MC signal yield assuming the SM branching fractions in Ref. [2], and N_B is the expected background yield.

The dominant background arises from continuum events ($e^+e^- \to q\overline{q}(\gamma)$), where the accidental combination of a ρ or ω candidate with a photon forms a B candidate. We suppress this background using the following quantities: (1) $\mathcal{F}$, a Fisher discriminant [7] constructed from 16 modified Fox-Wolfram moments [8, 9] and the scalar sum of the transverse momentum of all charged tracks and photons. (2) $\cos\theta^*_B$, where θ^*_B is the c.m. polar angle of the B candidate direction: true B mesons follow a $1-\cos^2\theta^*_B$ distribution, while candidates in the continuum background are uniformly distributed. (3) Δz, the separation between the decay vertex of the candidate B meson and the origin of the remaining tracks in the event along the z-axis. The two vertices are reconstructed in about 85% of the $\rho^0\gamma$ and $\omega\gamma$ events. Discrimination is provided due to the displacement of the signal B decay vertex from the other B, as tracks from continuum events typically have a common vertex. (4) A tagging quality r which indicates the level of confidence in the B-flavor determination described in Ref. [10]. The algorithm provides additional discrimination between signal and continuum background where no true B meson is present.

For each of the quantities $\mathcal{F}$, $\cos\theta^*_B$ and Δz, we construct one-dimensional likelihood distributions for signal and continuum events. Signal distributions are modeled with an asymmetric Gaussian function for $\mathcal{F}$, $\frac{3}{2}(a_0 - a_2\cos^2\theta^*_B)$ for $\cos\theta^*_B$, and an exponential convolved with a Gaussian resolution function for Δz. Continuum background distributions are modeled with an asymmetric Gaussian for $\mathcal{F}$, $(b_0 - b_2\cos^2\theta^*_B)$ for $\cos\theta^*_B$, and a sum of three Gaussians with a common mean for Δz; the coefficients a_0, a_2, b_0 are close to unity while the coefficient b_2 is close to zero. The Δz likelihood distribution for continuum is determined from data in the sideband region 5.20 GeV/$c^2 < M_{\rm bc} <$ 5.24 GeV/c^2, $|\Delta E| < 0.3$ GeV; we treat the two subsets of the data separately, as the vertex resolution is improved in the subset with the 4-layer SVD. The $\mathcal{F}$ and $\cos\theta^*_B$ likelihood distributions are determined from MC samples.

We form product likelihoods $\mathcal{L}_s$ and $\mathcal{L}_c$ for signal and continuum background, respectively, from the likelihood distributions for $\mathcal{F}$, $\cos\theta^*_B$ and (where available) Δz, since these quantities are independent. In the plane $(r, \mathcal{R})$ defined by the tagging quality r and the likelihood ratio $\mathcal{R} = \mathcal{L}_s/(\mathcal{L}_s + \mathcal{L}_c)$, signal tends to populate the edges at $r = 1$ and $\mathcal{R} = 1$, while continuum tends to populate the edges at $r = 0$ and $\mathcal{R} = 0$. We select the events in a signal enriched region defined by $\mathcal{R} > \mathcal{R}_1$ for $r > r_1$, and $\mathcal{R} > 1 - \alpha(1 + r)$ for $r_2 < r < r_1$, where the parameters r_1, r_2, $\mathcal{R}_1$ and α are mode- and subset-dependent and are determined so that $N_S/\sqrt{N_S + N_B}$ is maximized (we use this quantity instead of $N_S/\sqrt{N_B}$ because of the limited size of the MC simulation sample used in this procedure). The values are $r_1 = 0.85$, $r_2 = 0.01$, $\mathcal{R}_1 = 0.8$ and $\alpha = 0.025$ for the first subset of the $\rho^0\gamma$ mode; similar values are used for the other subsets. We define the rest of the area as the background enriched region.

We consider the following B decay backgrounds: $B \to K^*\gamma$, other $B \to X_s\gamma$ processes, $B \to \rho\pi^0$ and $\omega\pi^0$, $B \to \rho\eta$ and $\omega\eta$, $B^- \to \rho^-\rho^0$, other charmless B decays, and the $b \to c$ transition. We find the $b \to c$ background to be negligible. The $B \to K^*\gamma$ background may mimic the signal decay $B \to \rho\gamma$ if the kaon from K^* is

misidentified as a pion. To suppress $B \to K^*\gamma$ events we calculate $M_{K\pi}$, where the kaon mass is assigned to one of the charged pion candidates, and reject the candidate if $M_{K\pi} < 0.96$ (0.92) GeV/c^2 for the $\rho^0\gamma$ ($\rho^-\gamma$) mode. The decay chain $\overline{B}^0 \to \overline{K}^{*0}\gamma$, $\overline{K}^{*0} \to K^0_S\pi^0$, $K^0_S \to \pi^+\pi^-$ has a small contribution to $\overline{B}^0 \to \omega\gamma$ due to the tail of the K^* Breit-Wigner lineshape. In addition, $B \to K^*\gamma$ and other $B \to X_s\gamma$ decays contribute to the background when the ρ and ω candidates are selected from a random combination of particles.

Charmless decays $B \to \rho\pi^0$, $\omega\pi^0$, $\rho\eta$, and $\omega\eta$ may mimic the signal if a photon from π^0 or $\eta \to \gamma\gamma$ decay is soft and undetected by the π^0/η veto. To suppress this background, we reject the candidate if $|\cos\theta_{\rm hel}| > 0.8$ (0.6) for the $\rho^0\gamma$ and $\omega\gamma$ ($\rho^-\gamma$) modes, where the helicity angle $\theta_{\rm hel}$ is the angle between the π^+ and B momentum vectors in the ρ rest frame, or the angle between the normal to the ω decay plane and the B momentum vector in the ω rest frame. The decay $B^- \to \rho^-\rho^0$, $\rho^- \to \pi^-\pi^0$ also contributes to the $B^0 \to \rho^0\gamma$ mode when a pion from the ρ^- decay and a photon from the π^0 decay are both soft and undetected. Other charmless decays have very small contributions and are considered as an additional background component when we extract the signal yield.

The reconstruction efficiency for each mode is defined as the fraction of the signal yield remaining after all selection criteria, where the signal yield is determined from an extended unbinned maximum likelihood fit to the MC sample. Each signal distribution is modeled as the product of a Gaussian in $M_{\rm bc}$ and a Crystal Ball lineshape [11] in ΔE to reproduce the asymmetric ECL energy response for ΔE. The background component is modeled as the product of a linear function for ΔE and an ARGUS function [12] for $M_{\rm bc}$. The efficiencies are listed in Table I. The systematic error on the efficiency is the quadratic sum of the following contributions, estimated using control samples: the photon detection efficiency (2.2%) as measured in radiative Bhabha events; charged tracking efficiency (1.0% per track), from partially reconstructed $D^{*+} \to D^0\pi^+$, $D^0 \to K^0_S\pi^+\pi^-$, $K^0_S \to \pi^+(\pi^-)$; charged pion identification (1.0% per pion) from $D^{*+} \to D^0\pi^+$, $D^0 \to K^-\pi^+$; neutral pion detection (4.6–7.3%) from η decays to $\gamma\gamma$, $\pi^+\pi^-\pi^0$ and $3\pi^0$; $\mathcal{R}$-r and π^0/η veto requirements (5.4%) from $B^- \to D^0\pi^-$, $D^0 \to K^-\pi^+$; and uncertainty due to limited MC statistics (0.9–1.5%).

We perform an unbinned maximum likelihood fit to the data in the ($M_{\rm bc}$, ΔE) region bounded by $|\Delta E| < 0.3$ GeV and $M_{\rm bc} > 5.2$ GeV/c^2, simultaneously for the three signal modes and the two $B \to K^*\gamma$ modes; the latter are used to determine the residual $K^*\gamma$ backgrounds in the signal modes. We fit the two data subsets simultaneously, so that in total ten distributions are included in the fit. We define the combined branching fraction $\mathcal{B}(B \to (\rho,\omega)\gamma) \equiv \mathcal{B}(B^- \to \rho^-\gamma)$, assuming the isospin relation [13] $\mathcal{B}(B^- \to \rho^-\gamma) = 2\frac{\tau_{B^+}}{\tau_{B^0}}\mathcal{B}(\overline{B}^0 \to \rho^0\gamma) = 2\frac{\tau_{B^+}}{\tau_{B^0}}\mathcal{B}(\overline{B}^0 \to \omega\gamma)$; we use $\frac{\tau_{B^+}}{\tau_{B^0}} = 1.086 \pm 0.017$ [14]. We also assume $\mathcal{B}(B \to K^*\gamma) \equiv \mathcal{B}(B^- \to K^{*-}\gamma) = \frac{\tau_{B^+}}{\tau_{B^0}}\mathcal{B}(\overline{B}^0 \to \overline{K}^{*0}\gamma)$.

We describe the events in the fit region using a sum of functions for the signal, continuum, $K^*\gamma$, and other background hypotheses. Signal parameters for $M_{\rm bc}$ and ΔE are calibrated using $B^- \to D^0\pi^-$ and $B \to K^*\gamma$ samples, respectively. We use the combined branching fractions $B \to (\rho,\omega)\gamma$ and $B \to K^*\gamma$ as free parameters. The continuum background is modeled as the product of a linear function in ΔE whose slope is allowed to float, and an ARGUS function in $M_{\rm bc}$ whose parameters are fixed from a comparison between data and MC in the background enriched region and MC in the signal enriched region. The continuum contribution in the data is allowed to float. The size of the $K^*\gamma$ background component in each $(\rho,\omega)\gamma$ channel is constrained using the fit to the $K^*\gamma$ events. The levels of the other backgrounds are fixed using known branching fractions or upper limits.

Results of the fit are shown in Fig. 2 and listed in Table I. The significance of the fit, $\sqrt{-2\ln(\mathcal{L}_0/\mathcal{L}_{\rm max})}$, is found to be 1.2σ; where $\mathcal{L}_{\rm max}$ ($\mathcal{L}_0$) is the maximum likelihood from the fit when the signal branching fraction is floated (set to zero). To include the effect of possible systematic error in this calculation, we change each parameter by $\pm1\sigma$ in the direction that gives the smaller resulting significance. The systematic error in the signal yield is estimated by varying each of the fixed parameters by 1σ, and then taking the quadratic sum of the deviations in the signal yield from the nominal value. The combined branching fraction is $\mathcal{B}(B \to (\rho,\omega)\gamma) = (0.72\,^{+0.43}_{-0.39} \pm 0.28) \times 10^{-6}$, where the first and second errors are statistical and systematic, respectively.

Since the significance is small, we quote a 90% confidence level upper limit $\mathcal{B}_{90}$ using the formula $\int_0^{\mathcal{B}_{90}} \mathcal{L}(x)dx = 0.9\int_0^{\infty} \mathcal{L}(x)dx$, where $\mathcal{L}(x)$ is the likelihood function with the branching fraction fixed at x. The systematic error is taken into account assuming a Gaussian distribution. We find $\mathcal{B}(B \to (\rho,\omega)\gamma) < 1.4 \times 10^{-6}$ at the 90% confidence level. We also perform individual fits to the three signal modes; the corresponding upper limits are listed in Table I.

A similar fit is performed using the ratio of branching fractions $\mathcal{B}(B \to (\rho,\omega)\gamma)/\mathcal{B}(B \to K^*\gamma)$ instead of $\mathcal{B}(B \to (\rho,\omega)\gamma)$, so that the systematic error partially cancels. We find $\mathcal{B}(B \to (\rho,\omega)\gamma)/\mathcal{B}(B \to K^*\gamma) < 0.035$ at the 90% confidence level. One can use this result to constrain V_{td}: for example, using the prescription given in Ref. [15], $\frac{\mathcal{B}(B\to(\rho,\omega)\gamma)}{\mathcal{B}(B\to K^*\gamma)} = \left|\frac{V_{td}}{V_{ts}}\right|^2 \frac{(1-m^2_{(\rho,\omega)}/m^2_B)^3}{(1-m^2_{K^*}/m^2_B)^3}\zeta^2[1 + \Delta R]$ where the form factor ratio $\zeta = 0.85 \pm 0.10$ and $SU(3)$-breaking effect $\Delta R = 0.1 \pm 0.1$, we obtain $|V_{td}/V_{ts}| < 0.22$ at the 90% confidence level. This limit is slightly smaller than that resulting from searches for B_s mixing [14].

In conclusion, we search for the $b \to d\gamma$ process using

a simultaneous fit to the $B \to (\rho,\omega)\gamma$ and $B \to K^*\gamma$ modes. The upper limit we obtain is within the range of SM predictions [2, 3] and can be used to constrain $|V_{td}/V_{ts}|$.

We thank the KEKB group for the excellent operation of the accelerator, the KEK cryogenics group for the efficient operation of the solenoid, and the KEK computer group and the NII for valuable computing and SuperSINET network support. We acknowledge support from MEXT and JSPS (Japan); ARC and DEST (Australia); NSFC (contract No. 10175071, China); DST (India); the BK21 program of MOEHRD and the CHEP SRC program of KOSEF (Korea); KBN (contract No. 2P03B 01324, Poland); MIST (Russia); MHEST (Slovenia); SNSF (Switzerland); NSC and MOE (Taiwan); and DOE (USA).

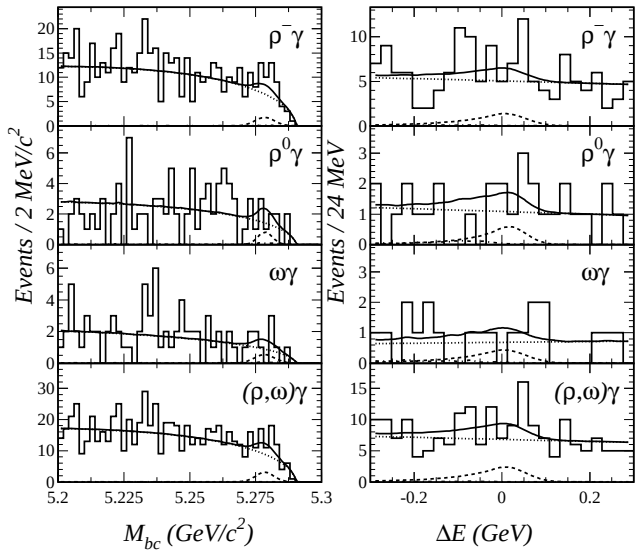

FIG. 2: Projections of the simultaneous fit results to $M_{\rm bc}$ (in the region -0.10 GeV $< \Delta E <$ 0.08 GeV) and ΔE (in the region 5.273 GeV/c^2 $< M_{\rm bc} <$ 5.285 GeV/c^2) for the individual modes and their sum. Lines represent the total fit result (solid), signal (dashed), continuum (dotted), and B decay background (dot-dashed) components.

[1] BaBar Collaboration, B. Aubert *et al.*, Phys. Rev. Lett. **94**, 011801 (2005).
[2] A. Ali and A. Ya. Parkhomenko, Eur. Phys. J. C **23**, 89 (2002).
[3] In addition to Ref. [2], for example, S. Bosch and G. Buchalla, Nucl. Phys. B **621**, 459 (2002); T. Huang, Z. Li and H. Zhang, J. Phys. G **25**, 1179 (1999).
[4] S. Kurokawa and E. Kikutani, Nucl. Instrum. Meth. A **499**, 1 (2003).
[5] Belle Collaboration, A. Abashian *et al.*, Nucl. Instrum. Meth. A **479**, 117 (2002).
[6] Y. Ushiroda, Nucl. Instrum. Meth. A **511**, 6 (2003).
[7] R. A. Fisher, Ann. Eugen. **7**, 179 (1936).
[8] Belle Collaboration, S.H. Lee *et al.*, Phys. Rev. Lett. **91**, 261801 (2003).
[9] G. C. Fox and S. Wolfram, Phys. Rev. Lett. **41**, 1581 (1978).
[10] H. Kakuno *et al.*, Nucl. Instrum. Meth. A **533**, 516 (2004).
[11] Crystal Ball Collaboration, J. E. Gaiser *et al.*, Phys. Rev. D **34**, 711 (1986).
[12] ARGUS Collaboration, H. Albrecht *et al.*, Phys. Lett. B **241**, 278 (1990).
[13] A. Ali, V. M. Braun and H. Simma, Z. Phys. C **6**, 437 (1994).
[14] Particle Data Group, S. Eidelman *et al.*, Phys. Lett. B **592**, 1 (2004).
[15] A. Ali, E. Lunghi and A. Parkhomenko, Phys. Lett. B **595**, 323 (2004).

TABLE I: Yield, significance (including systematic error), efficiency and fitted branching fraction (central value and 90% confidence level upper limit) for each mode and for $B \to (\rho, \omega)\gamma$.

				Branching Fraction	
Mode	Yield	Significance	Efficiency	Central Value	Upper Limit
$B^- \to \rho^-\gamma$	$18.7\,^{+10.1}_{-\ 9.2}$	1.7σ	$(5.5 \pm 0.4)\%$	$(1.24\,^{+0.67}_{-0.61} \pm 0.26) \times 10^{-6}$	2.2×10^{-6}
$\overline{B}^0 \to \rho^0\gamma$	$1.9\,^{+2.8}_{-2.7}$	0.3σ	$(3.9 \pm 0.3)\%$	$(0.18\,^{+0.33}_{-0.25} \pm 0.10) \times 10^{-6}$	0.8×10^{-6}
$\overline{B}^0 \to \omega\gamma$	$0.9\,^{+4.2}_{-3.3}$	0.1σ	$(3.9 \pm 0.4)\%$	$(0.08\,^{+0.39}_{-0.31} \pm 0.19) \times 10^{-6}$	0.8×10^{-6}
Combined	—	1.2σ	—	$(0.72\,^{+0.43}_{-0.39} \pm 0.28) \times 10^{-6}$	1.4×10^{-6}